Reconstituting Corticostriatal Network on-a-Chip Reveals the Contribution of the Presynaptic Compartment to Huntington's Disease

Amandine Virlogeux, Eve Moutaux, Wilhelm Christaller, Aurelie Genoux, Julie Bruyère, Elodie Fino, Benoît Charlot, Maxime Cazorla, Frédéric Saudou

Article

Cell Reports

Reconstituting Corticostriatal Network on-a-Chip Reveals the Contribution of the Presynaptic Compartment to Huntington's Disease

Graphical Abstract

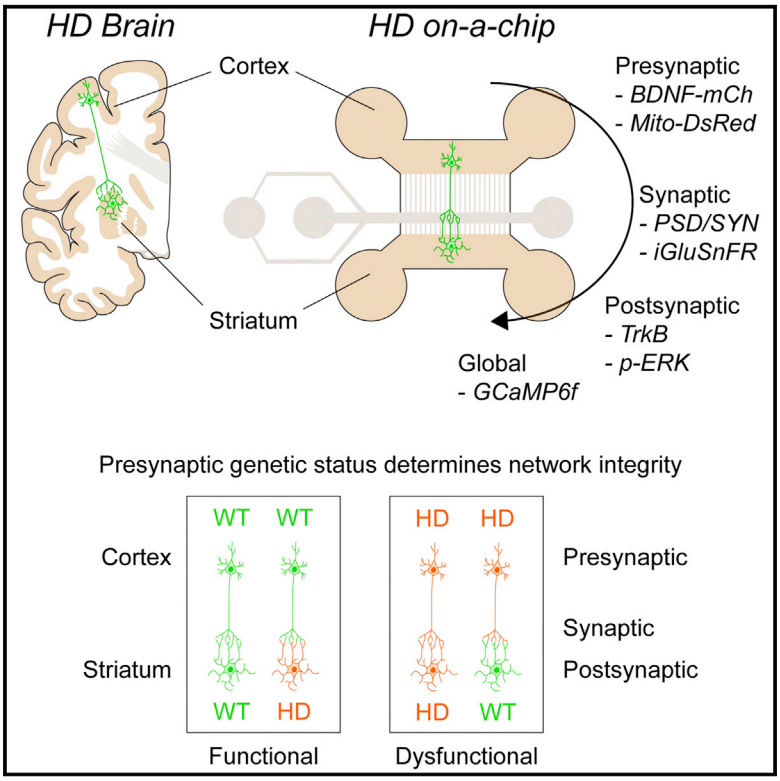

Highlights

- Microfluidic devices allow reconstitution of healthy and HD neuronal networks
- High-resolution imaging in HD mature networks shows pre- and postsynaptic defects
- HD corticostriatal network is defective and hypersynchronized
- Genetic status of presynaptic neurons determines functionality of the network

Authors

Amandine Virlogeux, Eve Moutaux, Wilhelm Christaller, ..., Benoit Charlot, Maxime Cazorla, Frédéric Saudou

Correspondence

frederic.saudou@inserm.fr

In Brief

Using microfluidics to reconstruct a Huntington's disease corticostriatal network, Virlogeux et al. identify recurrent pre- and postsynaptic alterations leading to global circuit dysfunctions and hypersynchrony. They further demonstrate that the genetic status of the presynaptic compartment determines integrity of the network.

Virlogeux et al., 2018, Cell Reports *22*, 110–122
January 2, 2018
https://doi.org/10.1016/j.celrep.2017.12.013

CellPress

OPEN ACCESS
CellPress

Cell Reports
Article

Reconstituting Corticostriatal Network on-a-Chip Reveals the Contribution of the Presynaptic Compartment to Huntington's Disease

Amandine Virlogeux,[1,2,3] Eve Moutaux,[1,2] Wilhelm Christaller,[1,2] Aurélie Genoux,[1,2] Julie Bruyère,[1,2] Elodie Fino,[1,2] Benoit Charlot,[4,5] Maxime Cazorla,[1,2] and Frédéric Saudou[1,2,6,7,*]
[1]Grenoble Institut des Neurosciences, Univ. Grenoble Alpes, 38000 Grenoble, France
[2]INSERM, U1216, 38000 Grenoble, France
[3]Faculté de Médecine, Univ. Paris Sud11, 94276 Le Kremlin-Bicêtre, France
[4]CNRS UMR5214, Institut d'Electronique et des Systèmes, 34000 Montpellier, France
[5]Univ. Montpellier, 34000 Montpellier, France
[6]CHU Grenoble Alpes, 38000 Grenoble, France
[7]Lead Contact
*Correspondence: frederic.saudou@inserm.fr
https://doi.org/10.1016/j.celrep.2017.12.013

SUMMARY

Huntington's disease (HD), a devastating neurodegenerative disorder, strongly affects the corticostriatal network, but the contribution of pre- and postsynaptic neurons in the first phases of disease is unclear due to difficulties performing early subcellular investigations *in vivo*. Here, we have developed an *on-a-chip* approach to reconstitute an HD corticostriatal network *in vitro*, using microfluidic devices compatible with subcellular resolution. We observed major defects in the different compartments of the corticostriatal circuit, from presynaptic dynamics to synaptic structure and transmission and to postsynaptic traffic and signaling, that correlate with altered global synchrony of the network. Importantly, the genetic status of the presynaptic compartment was necessary and sufficient to alter or restore the circuit. This highlights an important weight for the presynaptic compartment in HD that has to be considered for future therapies. This disease-on-a-chip microfluidic platform is thus a physiologically relevant *in vitro* system for investigating pathogenic mechanisms and for identifying drugs.

INTRODUCTION

Huntington's disease is a devastating inherited neurological disorder with late-onset manifestations including involuntary movements and psychiatric and cognitive symptoms. Neuropathology includes the selective dysfunction and neurodegeneration of medium spiny neurons from the striatum and of specific cortical neurons within the cerebral cortex. Several pathogenic mechanisms potentially contributing to Huntington's disease (HD) have been described (Ross and Tabrizi, 2011; Saudou and Humbert, 2016). In particular, early defects in the corticostriatal circuitry with alteration of pre- and/or postsynaptic compartments have been consistently reported (Saudou and Humbert, 2016; Zuccato et al., 2010). In support, the development of several animal models that recapitulate the clinical features of HD led to the observation of synaptic alterations, revealing potential defects in neuronal connectivity (Cepeda et al., 2003; Gatto et al., 2015). Also, fMRI in presymptomatic patients revealed early alteration of cortex and striatum as well as defects in connectivity (Rosas et al., 2010; Tabrizi et al., 2011). Although it is now clear that both cortical and striatal neurons participate in the pathogenic process, their exact contributions to the early process of neuronal dysfunction is debated.

Elegant *in vivo* studies aiming at reducing the expression of transgenic mutant polyQ-HTT in either cortical or striatal neurons of mice that express full-length human mutant HTT from a bacterial artificial chromosome transgene (BACHD) suggested that both compartments were contributing to late degeneration (Wang et al., 2014). However, the cortical and striatal promoters used in this study only partially reduced mutant polyQ-HTT expression, and the cortical promoter was not selective since it also reduced striatal expression. To circumvent the difficulties of such *in vivo* experiments and study early dysfunction processes, strategies using co-culturing of cortical and striatal cultures in dishes have been reported (Buren et al., 2016). These primary neurons resemble the *in vivo* environment more closely than cell lines, but their random distribution in culture may lead to the creation of nonspecific, multidirectional, uncontrolled connections between the two populations, making it difficult to interpret the mechanisms involved in the disease. There is, therefore, a crucial need to develop more physiological and controlled contexts for reproducing the corticostriatal connections found *in vivo* while keeping subcellular resolution for studying the early mechanisms underlying neuronal dysfunction.

Here we present a microfluidic platform for the *in vitro* reconstruction of healthy and HD networks in which each neuronal compartment (presynaptic, synaptic, and postsynaptic) is identified (space compartmentalization) and in which the progression from axonal growth to synapse regulation is controlled (time compartmentalization). This microfluidic device is compatible with high-resolution videomicroscopy for studying intracellular

dynamics selectively in each compartment as well as global circuit functioning. We built a fluidically isolated corticostriatal network using neurons from an HD mouse model to investigate alterations in presynaptic dynamics, synaptic morphology and transmission, postsynaptic trafficking and signaling, as well as their consequences on global network dynamics in the pathological context of HD. Surprisingly, we found that presynaptic dysfunctions are necessary and sufficient to generate various pathological features within the striatal compartment, suggesting that cortical defects may be critical to the progression of the disease. Conversely, wild-type cortical neurons are sufficient to restore cellular alterations in mutant striatal neurons, suggesting that the manipulation of cortical neurons may be sufficient to achieve therapeutic effects. This disease-on-a-chip platform may, therefore, be useful not only for investigating pathogenic mechanisms but also for testing drugs of interest for HD treatment. The versatility of the device makes it suitable for use in other neurological disorders characterized by network or synapse dysfunction.

RESULTS

Space and Time Compartmentalization of Healthy and HD Corticostriatal Networks *In Vitro*

We reconstructed an *in vitro* corticostriatal network for subcellular investigations using the previous generation of polydimethylsiloxane (PDMS) microfluidic devices, which allow the access and manipulation of synapses and their pre- and postsynaptic compartments independently (Taylor et al., 2010). We modified the device to optimize fluidic isolation and to reduce the number of axons and dendrites to a unique branch in each channel by reducing their width to 3 μm (Figure S1A). The device consisted of two neuronal chambers (each containing either cortical or striatal neurons) connected via an intermediate synaptic chamber (containing corticostriatal synapses) through microchannels of different lengths (500 μm for cortical neurons and 75 μm for striatal neurons) (Figures 1A and S1A). The dendrites cannot grow to lengths of more than 450 μm (Taylor et al., 2005), so only axons from cortical neurons can reach the synaptic compartment (Figure 1B). By contrast, the 75-μm-long microchannels emerging from the striatal compartment do not discriminate between axons and dendrites, making it possible for striatal dendrites to come into contact with cortical axons.

We limited the number of striatal axons reaching the synaptic chamber, by generating a gradient of laminin from the cortical chamber to the striatal chamber, while keeping the poly-D-lysine concentration constant. This gradient helped to keep striatal axons away from the synaptic compartment, thus preventing non-physiological striatocortical contacts. In an effort to mimic physiological corticostriatal projections, we enriched the cortical chamber with CTIP2-/TBR1-positive neurons by performing primary cultures at embryonic day (E)15.5 (Digilio et al., 2015) (Figure S1B). These neurons corresponded to the deepest layers of the cortex (i.e., layers V and VI) that send axons to subcortical targets such as the striatum. Axons from cortical neurons crossed the channels by 3 days *in vitro* (DIV 3), and they began making contacts with striatal dendrites in the synaptic chamber at around DIV 5. The synaptic chamber, which was devoid of neuronal cells (Figure S1C), was progressively enriched in mature corticostriatal synaptic contacts until DIV 14, as shown by the juxtaposition of the presynaptic marker synaptophysin and the postsynaptic marker PSD95 that reached a density of 108.2 ± 9.2 contacts/100 μm (n = 27 fields) (Figures 1C and S1D). Glial Fibrillary Acidic Protein (GFAP)-positive branches were also found around neurites and synaptic contacts in the synaptic chamber, consistent with the formation of tripartite synapses among axons, dendrites, and glial cells (Figure 1D).

Because cortical neurons were mostly glutamatergic, we determined the functionality of corticostriatal synapses by lentiviral expression of the glutamate sensor iGluSnFR in the striatal chamber (Marvin et al., 2013). We found that the synaptic contacts were fully mature by DIV 14, as shown by the number of fluorescent spots that reached a plateau at 109,300 ± 6,726/mm^2 (n = 25 fields) in the synaptic chamber after stimulation of cortical neurons with glycine/strychnine treatments (Figure 1E). To study corticostriatal network connectivity, we infected striatal neurons with GCaMP6f, a fast genetically encoded calcium sensor that reliably detects single action potentials (Chen et al., 2013), and we recorded spontaneous neuronal activity. We found that around 83% of striatal cells elicited spontaneous and synchronized episodes of bursting activity at DIV 14 (Figure 1F). At DIV 14, the number of GCaMP6f events was 6.3 ± 0.1/cell/30 s, and 47.5% ± 14.6% of them were highly synchronized (n = 751 cells) and remained constant (Movie S1), consistent with matured neuronal cultures (Chiappalone et al., 2006). These observations demonstrate the efficacy of this device for reproducing a physiological corticostriatal network *in vitro* in which cortical neurons progressively form unilateral synapses with striatal neurons via oriented axodendritic contacts surrounded by astrocytes.

To study cellular and global dysfunctions in the diseased network, we used cortical and striatal neurons from heterozygous mice carrying a 140 CAG repeat in the mouse *Htt* gene (Menalled et al., 2002) (*Hdh*$^{CAG140/+}$, referred to here as HD mice). We did not notice major differences in the establishment of wild-type and HD networks in the device. We then studied multiple cellular alterations using a palette of selective markers in each compartment to evaluate presynaptic dynamics, synaptic morphology and transmission, postsynaptic responses, as well as the global consequences on network activity.

Axonal Transport of Vesicles Is Reduced in the Mature HD Network

To study presynaptic alterations in corticostriatal projecting neurons, we analyzed axonal transport of Brain-Derived Neurotrophic Factor (BDNF)-containing dense-core vesicles (DCVs) because it is critically impaired in HD (Gauthier et al., 2004). We investigated the transport of BDNF in cortical axons at the following different stages of neuronal maturation: early (DIV 4, before synaptic contacts), intermediate (DIV 10, immature synaptic contacts), and late (DIV 18, mature synaptic contacts), using neurons from the HD mouse model (Menalled et al., 2002). To do so, cortical neurons were infected with a lentivirus expressing mCherry-tagged BDNF (BDNF-mCh) at DIV 1 (Hinckelmann et al., 2016).

Fast video acquisitions were performed in the bottom part of axonal microchannels to select for axonal transport without

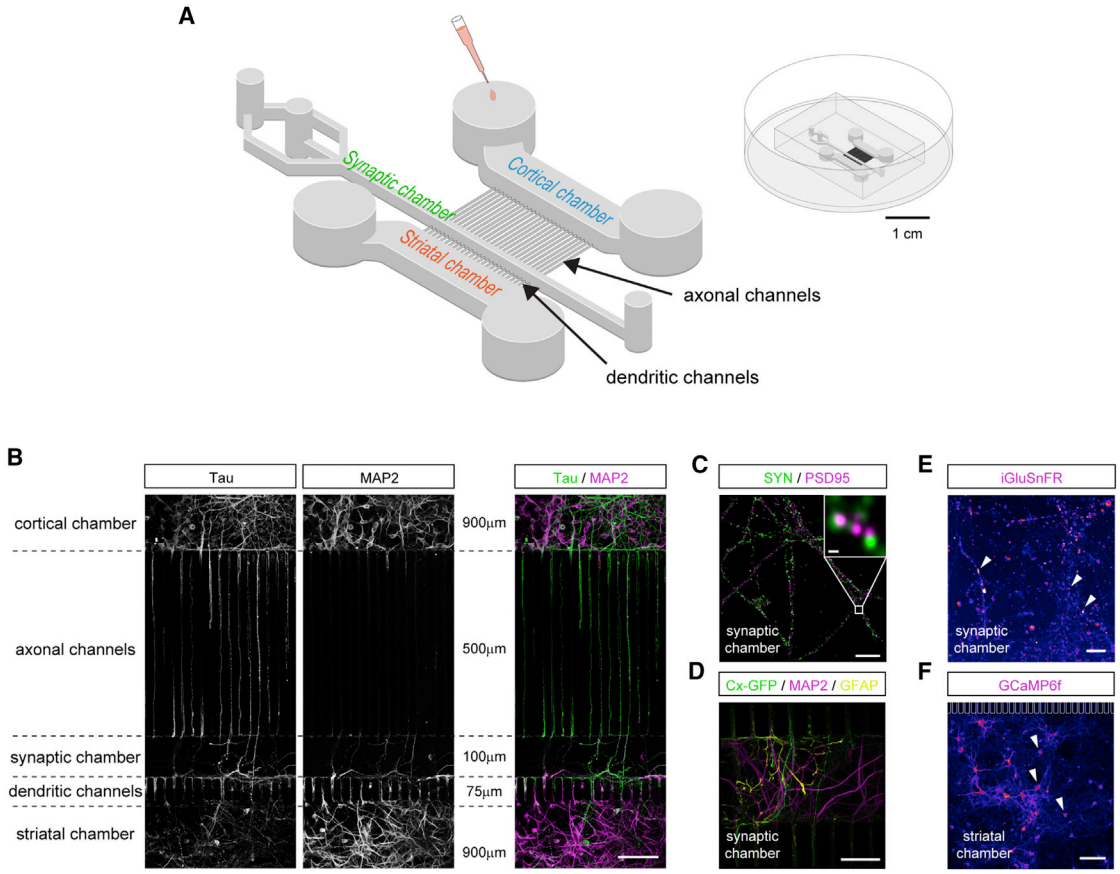

Figure 1. *In Vitro* Reconstruction of Corticostriatal Network Using Microfluidics

(A) Schematic of the 3-compartment microfluidic device allowing fluidic isolation of cortical and striatal chambers that are connected via microchannels and an intermediate synaptic chamber. Cylinders represent accessible wells for seeding neurons and/or perfusing liquids (culture medium or drugs). Microchannels are different in length to allow axons from cortical neurons and dendrites from striatal neurons to reach the synaptic chamber. Inset shows silicon microfluidics fixed to a microscopy-compatible glass-bottom microdish.

(B) Cortical axons connect striatal dendrites in the synaptic chamber. Axons (Tau positive), but not dendrites (MAP2 positive), from cortical neurons cross the 500-μm-long axonal channels to reach the synaptic and striatal chambers. Conversely, dendrites from striatal neurons reach the synaptic chamber by crossing the 75-μm-long dendritic channels, while axons are preferentially kept away using a gradient of coating. Scale bar, 100 μm.

(C) Adjacent spots of synaptophysin (SYN, presynaptic marker) and PSD95 (postsynaptic marker) show the formation of synaptic contacts between cortical axons and striatal dendrites in the synaptic chamber. Scale bar, 10 μm (inset, 200 nm).

(D) Striatal astrocytes (GFAP) grow extensions into the synaptic chamber that surround contacts between cortical axons (Cx-GFP) and striatal dendrites (MAP2). Scale bar, 50 μm.

(E) Efficient glutamate release (iGluSnFR) from projecting cortical axons confirms functional corticostriatal connections in the synaptic chamber at DIV 14. White arrows show glutamate release sites. Scale bar, 20 μm.

(F) Calcium imaging (GCaMP6f) shows high, synchronized neuronal activity in striatal neurons at DIV 14. White arrows indicate active neurons. Scale bar, 100 μm. See also Figure S1 and Movie S1.

dendritic contamination. Acquisitions were performed longitudinally using the same microfluidics at DIV 4, 10, and 18 (Figures 2A–2C and S2A; Movie S2). Segmental velocities and the number of vesicles were reduced in both anterograde and retrograde directions in HD neurons, suggesting that, in addition to a defect in axonal transport per se, vesicle synthesis was also altered in HD. This finding is consistent with previous reports of defects in trafficking from the endoplasmic reticulum to the Golgi apparatus and the plasma membrane in neurons from HD mouse models (Borrell-Pagès et al., 2006; Gauthier et al., 2004). The shift in the distribution of velocities and number of vesicles (Figure 2C) had a striking effect on the global linear flow rate of vesicle trafficking in axons and on the net flux, with half as much anterograde transport. These defects were already present at the early stage, as previously reported in other studies on immature free cultures (Gauthier et al., 2004; Her and Goldstein, 2008), but they became increasingly marked as the system matured.

Mitochondrial Fragmentation and Motility Increase in Mature Presynaptic HD Axons

Studies on the dynamics of mitochondria in the context of HD have yielded conflicting results (Gauthier et al., 2004; Trushina et al., 2004). We therefore investigated the axonal dynamics of

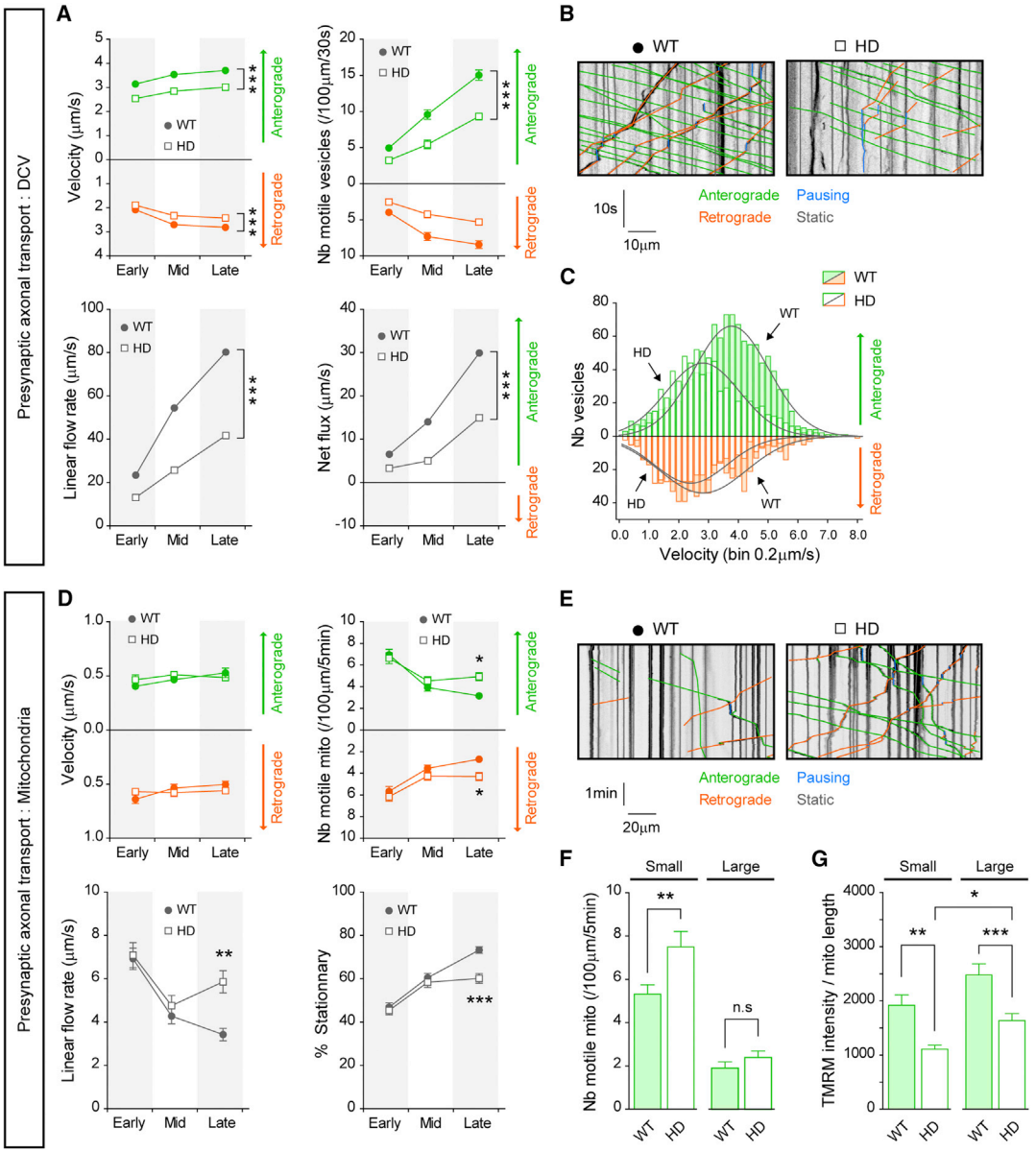

Figure 2. Progressive Dysfunctions of Presynaptic Dynamics in the HD Network

(A–C) Impaired axonal trafficking of DCVs (BDNF-mCh) from early to late neuronal maturation in HD.

(A) Kinetics analyses show altered axonal transport of motile vesicles in *Hdh*$^{CAG140/+}$ (HD) neurons compared to wild-type (WT) neurons at every stage of network maturation: decreased velocities (anterograde, $F_{1,490} = 96.3$, ***$p < 0.0001$; retrograde, $F_{1,490} = 24.4$, ***$p < 0.0001$; n = 82), number (anterograde, $F_{1,490} = 115.5$, ***$p < 0.0001$; retrograde, $F_{1,490} = 93.2$, ***$p < 0.0001$), net flux ($F_{1,490} = 215.8$, ***$p < 0.0001$), and linear flow rate ($F_{1,490} = 76.6$, ***$p < 0.0001$).

(B) Representative kymographs show DCV axonal trafficking obtained in WT and HD neurons at DIV 14.

(C) Changes in the distribution of motile vesicles in axons in HD neurons are compared to WT neurons at DIV 14 (anterograde, $X^2 = 86.7$, $p < 0.0001$; retrograde, $X^2 = 28.5$, $p < 0.0001$).

(D–G) Late alterations in mitochondria dynamics and fission (Mito-DsRed) in HD.

(D) Kinetics analyses show no defect in velocity at any stage of network maturation but show alterations at the latest stage: increased motility (late versus early: anterograde, *$p < 0.05$; retrograde, *$p < 0.05$; n = 70) and decreased proportion of stationary mitochondria (***$p < 0.001$) leading to increased linear flow rate (**$p < 0.01$), and in HD.

(E) Representative kymographs show mitochondria axonal trafficking obtained in WT and HD neurons at DIV 14.

(F) Increased number of small motile mitochondria in HD at DIV 14 (**$p < 0.01$; n = 32) indicates increased fission and motility at the latest stage of network maturation.

(G) Decreased TMRM signal in HD neurons, which indicates functional defects in mitochondria (**$p < 0.01$ and ***$p < 0.001$; n = 120), is more pronounced in small mitochondria (*$p < 0.05$). Error bar indicates SEM.

See also Figure S2 and Movies S2 and S3.

mitochondria in our reconstituted HD network (Figures 2D–2F and S2B; Movie S3). We found that the velocity of mitochondria was unaffected regardless of the stage of network maturation. By contrast, in the final stage of network maturation, we observed an increase in the number of motile mitochondria, resulting in a significant increase in the linear flow rate and a decrease in the proportion of stationary episodes. We then investigated the cause of this increase in the number of motile mitochondria in the mature network. We found that a large proportion of the motile mitochondria in the HD network were small, whereas the number of elongated mitochondria did not differ between wild-type and mutant neurons (Figures 2F and S2C). The increase in the number of small mitochondria, which are more mobile, in the context of HD, is consistent with the increase in mitochondrial fragmentation reported *in vitro* and *in vivo* (Costa et al., 2010; Song et al., 2011). We also measured mitochondrial membrane potential using tetramethylrhodamine, methyl ester (TMRM) labeling in wild-type (WT) and HD neurons to assess their functional integrity (Scaduto and Grotyohann, 1999). We found that both small and large mitochondria were functionally defective, as shown by the decrease in TMRM labeling (Figure 2G). Interestingly, the decrease in membrane potential was significantly more pronounced in small mitochondria compared to large ones. We conclude that, in contrast to the early defect in axonal transport of BDNF, alteration in mitochondria trafficking and function appears as a late event in the HD network.

The Corticostriatal Network Is Misconnected and Dysfunctional in HD

We next investigated possible changes in the structure and function of corticostriatal synapses in the mature HD circuit (>DIV 14). We assessed synapse density by quantifying the number of synaptophysin spots (presynaptic marker) adjacent to PSD95 spots (postsynaptic marker) in the synaptic chamber using high-resolution Airyscan confocal microscopy (Figures 3A and 3B). We found that the frequency of synaptophysin being located next to PSD95 was significantly lower in the HD corticostriatal network than in the WT network. The overall number of synaptic contacts was decreased in the HD network. The morphology of remaining contacts was changed, with a higher proportion of large and clustered presynaptic sites than in WT neurons (Figures 3C and 3D). We analyzed whether findings obtained in microfluidics could be observed in brain corticostriatal slices from HD mice. Using PSD95 as a postsynaptic marker and VGLUT1 as a selective presynaptic marker for cortical projections (McKinstry et al., 2014), we confirmed that the number of corticostriatal contacts was also decreased *in vivo* in the striatum of HD mice (Figure S3). These *in vivo* observations therefore validate our microfluidic platform as a predictive tool for detecting alterations in the corticostriatal pathway.

We next investigated whether the altered synaptic morphology affected the capacity of cortical neurons to release glutamate by infecting striatal neurons with iGluSnFR-expressing lentiviruses and performing live fluorescence acquisition on the synaptic chamber during the stimulation of cortical neurons with glycine/strychnine treatment (Figures 3E and 3F). We observed a significant decrease in the density of glutamate presynaptic release sites, as shown by the smaller number of iGluSnFR spots in the synaptic chamber. The remaining iGluSnFR-positive spots were significantly larger than those in WT conditions (Figure 3G), consistent with the larger size of the presynaptic clusters detected by immunostaining for synaptophysin. Abnormally large clusters of iGluSnFR and synaptophysin spots in presynaptic terminals suggest aberrant synaptic release of excitatory neurotransmitter, which would be in agreement with the observed increased excitatory release in HD flies (Romero et al., 2008).

HD Induces Defects in Postsynaptic Trafficking and Signaling

We then studied the postsynaptic striatal compartment by analyzing dendritic trafficking and signaling responses to cortical stimulation. We investigated the dynamics of dendritic vesicles containing tropomyosin-related kinase receptor B (TrkB), the receptor for BDNF. TrkB is endogenously expressed in striatal neurons, and defects in its trafficking and signaling capacity have been described in HD (Brito et al., 2014; Liot et al., 2013; Plotkin et al., 2014). Striatal neurons were infected with a lentivirus expressing a fully functional mCherry-tagged TrkB receptor (TrkB-mCh) and electroporated with a plasmid expressing MAP2-GFP, for the recording of TrkB vesicular dynamics specifically in dendrites (Figure 4A; Movie S4). Kymograph analyses were performed at DIV 14, when the network was mature (Figures 4B and S4A). In HD corticostriatal networks, the number of TrkB vesicles were reduced in both anterograde and retrograde directions, as previously reported in young immature cultures (Liot et al., 2013) (Figure 4C). These changes led to a large decrease in the global linear flow rate of vesicle trafficking in striatal dendrites.

We then investigated the consequences of altered synaptic transmission for postsynaptic signaling, using ERK phosphorylation as a readout of the striatal response to cortical stimulation (Figures S4B and S4C). We found a significant decrease in the number of phospho-ERK-immunopositive striatal neurons in response to cortical stimulation with glycine/strychnine treatments in the context of HD (Figures 4D and 4E). We confirmed the defect in the phospho-ERK-signaling pathway using western blotting analyses of striatal cell bodies extracted from the microfluidic platform (Figures 4F and 4G). Interestingly, we found that the decrease in postsynaptic phospho-ERK signaling preferentially affected enkephalin-positive striatal neurons (Figures S4D–S4F), which correspond to output-projecting neurons of the striatum that are particularly affected in HD (Saudou and Humbert, 2016). Thus, in addition to the presynaptic and synaptic defects, there were also profound changes to postsynaptic intracellular dynamics and signaling in the HD corticostriatal network.

Corticostriatal Connectivity Is Defective and Hypersynchronized in HD

We next studied the global consequences of these alterations on the global functioning of the network. To do so, we infected striatal neurons with an adeno-associated virus expressing GCaMP6f, and we analyzed spontaneous responses to cortical inputs (Movie S5). In WT neurons, we recorded sustained neuronal activity with numerous episodes of bursting activity and single asynchronous events within the network at DIV 10–14 (Figures 5A, S5A, and S5B). By contrast, HD neurons

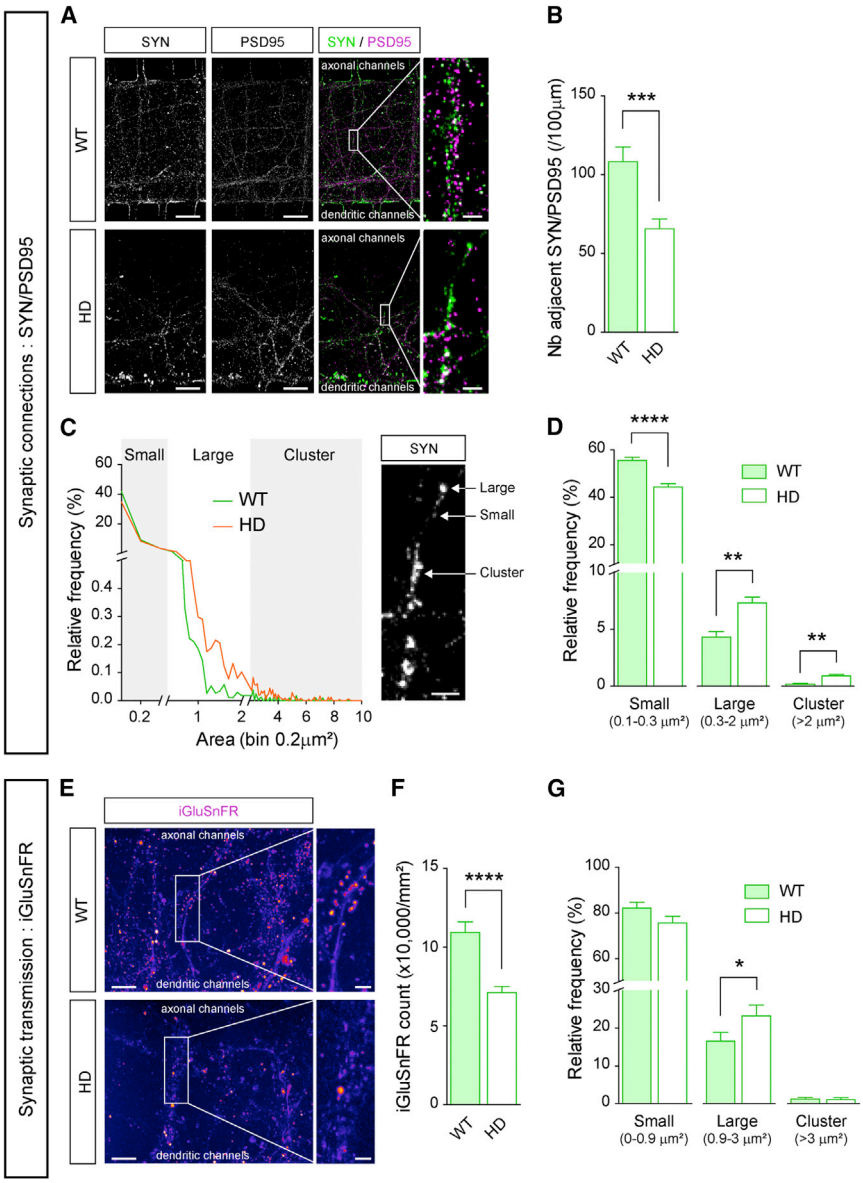

Figure 3. Impaired Synaptic Structure and Function in the HD Network

(A–D) Decreased synaptic connections in HD.

(A) Airyscan confocal images show SYN/PSD95 colocalization in the synaptic chamber of WT and HD corticostriatal network at DIV 14. Insets show 10× magnification of representative branches. Scale bars, 20 µm (insets, 2 µm).

(B) Quantification of the number of adjacent SYN/PSD95 spots per branches shows decreased synaptic connections in HD neurons (***$p < 0.001$; $n = 27$).

(C) Synaptophysin spots can be distributed based on their size and grouped into 3 categories: small (<0.3 µm^2), large (0.3–2 µm^2), and clustered (>2 µm^2), as shown in the inset. Scale bar, 2 µm.

(D) Quantification of synaptophysin spot size shows a decreased number of small, restricted synaptic sites and increased number of large and clustered sites in the HD network (**$p < 0.01$ and ****$p < 0.0001$; $n = 9$).

(E–G) Impaired glutamate transmission at corticostriatal synapses in HD.

(E) Images show iGluSnFR deflection in fluorescence in the synaptic chamber of WT and HD network at DIV 14 after chemical stimulation of cortical neurons. Insets show 4× magnification of striatal postsynaptic sites responding to presynaptic release of glutamate. Scale bars, 20 ìm (insets, 5 ìm).

(F) Quantification of the number of iGluSnFR spots per millimeter^2 shows decreased glutamate transmission sites between cortical and striatal neurons in HD (****$p < 0.0001$; $n = 25$).

(G) Quantification of iGluSnFR spot size shows fewer small, restricted transmission sites and an increased number of large, diffuse sites in the HD network (*$p < 0.05$; $n = 26$). Error bar indicates SEM.

See also Figure S3.

remained silent, as shown by the much smaller number of events than for WT striatal neurons (Figure 5B). However, although HD neurons were only half as active as WT neurons, they displayed highly synchronized bursting episodes separated by long phases of inactivity (Figure 5A; Movie S5). Furthermore, the amplitude of bursting episodes was three times higher than that in WT neurons (Figure 5C).

We then compared the occurrence of synchronous events between WT and HD neurons (Figures 5D and S5C). We found that only one-third of events were synchronized in WT neurons at this stage. By contrast, in HD neurons, this proportion increased to more than two-thirds, suggesting a dramatic functional reorganization of the corticostriatal network. This change in synchrony indicates that, while the system remains globally silent, sparse episodes of intense bursting transmission may occur at random and are propagated uniformly throughout the striatum. These findings may reflect the smaller number of functional synapses, together with the larger presynaptic clusters and glutamate release sites (Figure 3), potentially leading to the rare, but uncontrolled, massive release of neurotransmitters. We therefore conclude that, in HD, the corticostriatal network reorganizes into an abnormally overactive system that may propagate irrelevant cortical information, ultimately compromising the survival of striatal neurons.

The Genetic Status of the Presynaptic Compartment Determines Network Integrity

Several studies have highlighted the importance of autonomous defects within the striatum and of the contribution of both striatal and corticostriatal projecting neurons to circuit dysfunction and degeneration (Buren et al., 2016; Estrada-Sánchez et al., 2015; Wang et al., 2014; Plotkin et al., 2014). The fluidic isolation of the pre- and postsynaptic compartments, with an isolated

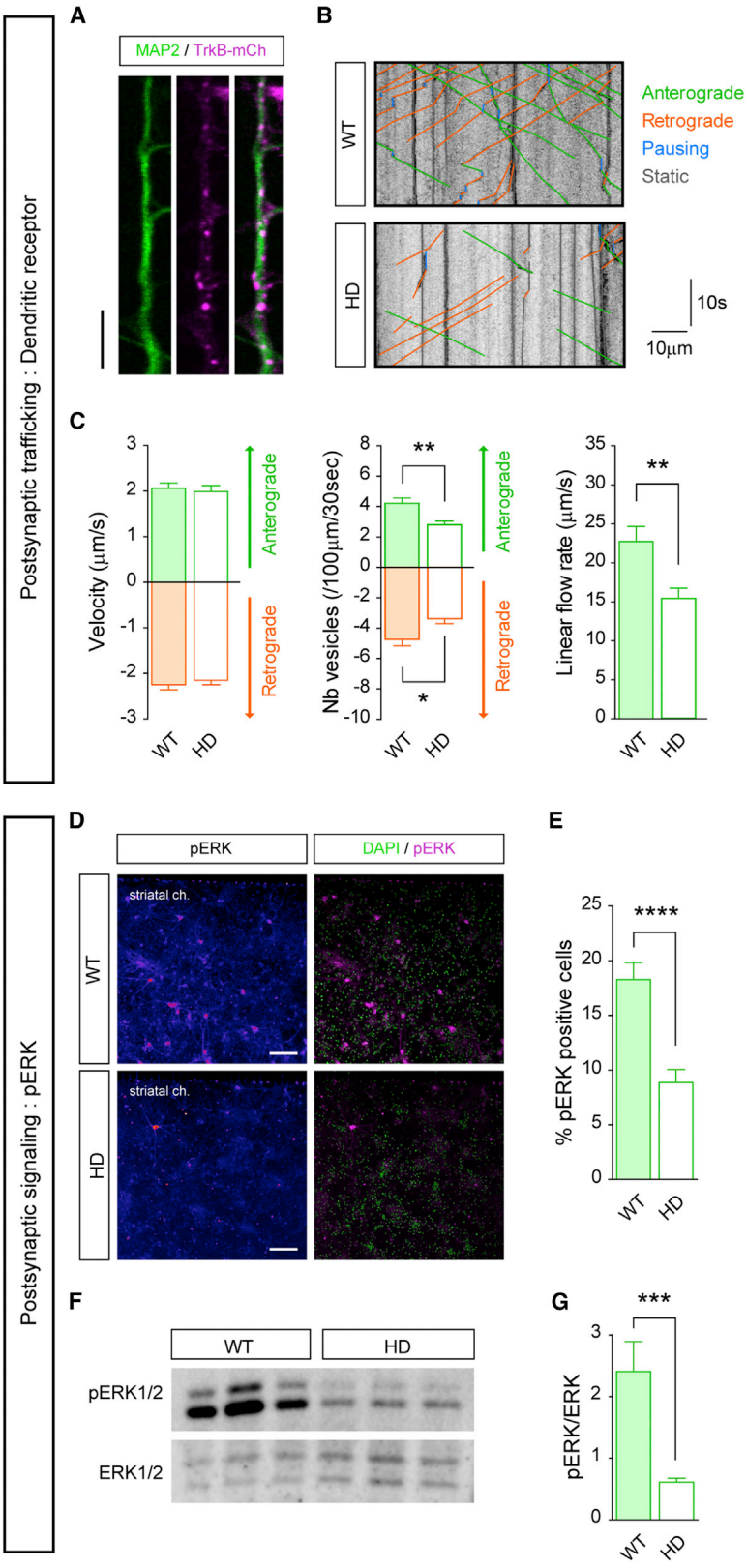

Figure 4. Alterations in Postsynaptic Dynamics and Signaling in HD Striatal Neurons

(A–C) Impaired dendritic trafficking (TrkB-mCh) in HD.

(A) Images taken from live-cell recordings show TrkB-mCh vesicles traveling in MAP2-positive dendrites of striatal neurons (see Movie S4). Scale bar, 10 μm.

(B) Representative kymographs show TrkB-mCh dendritic trafficking obtained in WT and HD neurons at DIV 14.

(C) Kinetics analysis of dendritic transport shows decreased numbers of anterograde and retrograde vesicles, leading to decreased global linear flow rate in HD neurons (*$p < 0.05$ and **$p < 0.01$; $n = 31$).

(D–G) Impaired phospho-ERK signaling in HD postsynaptic striatal neurons.

(D) Images show pERK immunofluorescence in the striatal chamber of WT and HD networks at DIV 14 after glycine/strychnine stimulation of cortical neurons. DAPI co-staining was used to evaluate the total number of neurons for quantification. Scale bars, 100 μm.

(E) Quantification of pERK-positive cells after cortical stimulation shows a decreased response in HD striatal neurons (****$p < 0.0001$; $n = 20$).

(F) Western blot of phospho- and total ERK1/2 from striatal neurons of WT and HD networks at DIV 14 after glycine/strychnine stimulation of cortical neurons is shown.

(G) Quantification of pERK/ERK bands after cortical stimulation shows a dramatic decrease in pERK signaling in HD striatal neurons (***$p < 0.001$; $n = 6$). Error bar indicates SEM. See also Figure S4 and Movie S4.

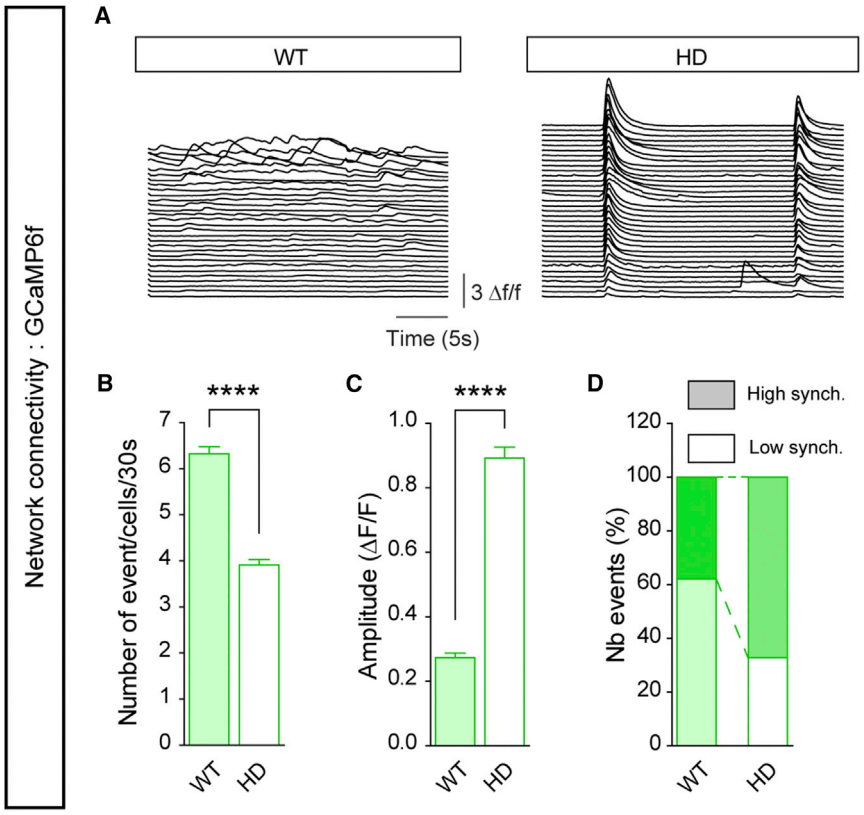

Figure 5. Dysfunctional Reorganization of Corticostriatal Connectivity and Synchrony in the HD Network

(A) Representative GCaMP6f fluorescent traces (one trace per neuron) obtained from WT and HD striatal neurons show the global reorganization of network activity in HD (see Movie S5).

(B–D) Quantifications of GCaMP6f dynamics show alterations at different levels of neuronal activity and synchrony in the HD network. (B) Decreased number of events per cells (****$p < 0.0001$; $n = 757$), (C) increased amplitude of response per event (****$p < 0.0001$), and (D) global increase in the proportion of highly synchronized events in HD striatal neurons compared to WT neurons (WT, 38.8%; HD, 67.1%) are shown. Error bar indicates SEM.

See also Figure S5 and Movie S5.

synaptic space, provided the opportunity to manipulate the genetic status of the cortical and striatal neurons independently within the reconstituted network. We therefore placed either WT or mutant *Hdh*$^{CAG140/+}$ neurons in both cortical and striatal compartments (WT-WT and HD-HD), or we used WT cortical neurons with mutant *Hdh*$^{CAG140/+}$ striatal neurons (WT-HD) or mutant *Hdh*$^{CAG140/+}$ cortical neurons with WT striatal neurons (HD-WT) (Figure 6A). We then investigated the contribution of each compartment to the observed network defects in our microfluidic device.

We investigated glutamate transmission, and we found that an HD-WT corticostriatal network was sufficient to recapitulate the deficits in transmission observed in a full HD-HD network (Figure 6B). By contrast, the WT-HD network closely resembled the full WT-WT network, suggesting that synaptic alterations are independent of the postsynaptic compartment in HD. We then measured ERK signaling within striatal neurons, as this striatal response is typically altered in HD (Brito et al., 2014; Liot et al., 2013; Plotkin et al., 2014). Surprisingly, HD striatal neurons displayed no phospho-ERK signal defect when the cortical neurons were WT (WT-HD network) (Figure 6C). By contrast, WT striatal neurons yielded defects similar to those of mutant neurons when the cortical neurons were HD (HD-WT network). These observations were confirmed using phospho-ERK western blotting analyses performed selectively from neuronal cell bodies of the striatal chamber (Figure 6D). Thus, presynaptic cortical neurons have a critical impact on the maintenance of striatal neurons, suggesting that the basal functioning and survival of striatal neurons depends on corticostriatal projections rather than on cell-autonomous mechanisms. We further analyzed global communication and synchrony between cortical and striatal neurons in all four genetic conditions, through the viral expression of GCaMP6f in striatal neurons. Again, we found that neuronal activity in the HD-WT network resembled that in the full HD-HD network (smaller number of events, a larger amplitude, and highly synchronized bursting events) (Figures 6E–6G). By contrast, WT presynaptic neurons were able to maintain correct connectivity and synchrony even when the striatal neurons were of the HD genotype in the WT-HD network.

To generalize our observations that presynaptic alterations are necessary and sufficient to induce synapse and network dysfunctions in HD, we repeated this set of experiments using another widely used HD mouse model. To do so, iGluSnFR, phospho-ERK, and GCamP6f analyses were performed using the heterozygous knockin *Hdh*$^{Q111/+}$ mice that express human *HTT* exon 1 sequence with 109 repeats of CAG (Wheeler et al., 1999). Using this model, we confirmed that the HD-WT configuration recapitulated dysfunctions observed in the full HD-HD network at the level of synaptic transmission (decreased iGluSnFR density), postsynaptic signaling (decreased phospho-ERK-positive cells and phospho-ERK western blot signal after cortical stimulation), and network connectivity (decreased number of GCaMP6f events, increased amplitude, and increased number of highly synchronized bursting events) (Figure S6). As previously observed with *Hdh*$^{CAG140/+}$ cultures, *Hdh*$^{Q111/+}$ striatal neurons showed no synaptic, postsynaptic, or synchrony dysfunctions when cortical neurons were of the WT genotype (WT-HD network) and resembled the full WT-WT configuration. We therefore conclude that the genetic status of the cortical neurons determines the function and dysfunction of the corticostriatal network in neurons from two mouse models of HD.

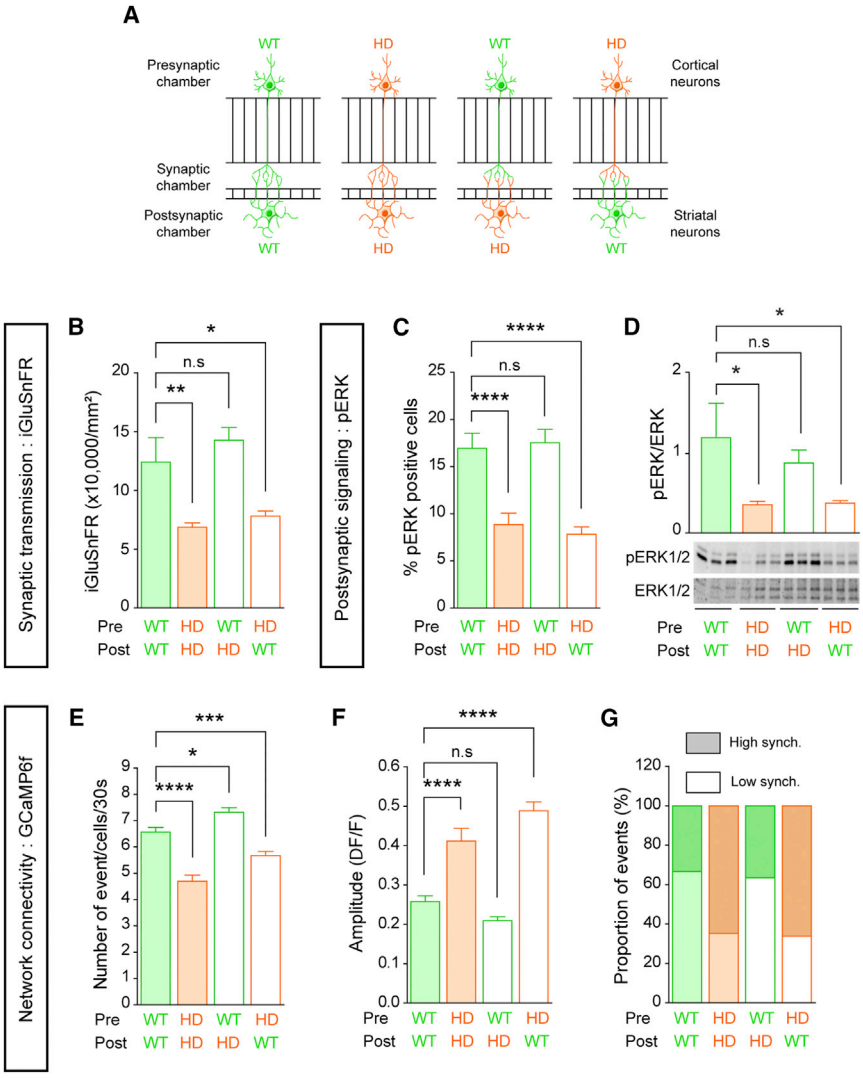

Figure 6. Selective Contribution of Pre- and Postsynaptic Compartments to Local and Global Dysfunctions in HD Neurons

(A) Strategy for manipulating the genetic status of presynaptic and postsynaptic neurons. Four combinations were tested: full WT (WT-WT), full HD (HD-HD), cortical WT + striatal HD (WT-HD), and cortical HD + striatal WT (HD-WT).

(B) Quantification of the number of iGluSnFR spots shows altered glutamate transmission ($F_{3,120} = 8.7$, $p < 0.0001$; n = 30) in the HD-HD network, which is fully recapitulated in the HD-WT condition (*p < 0.05 and **p < 0.01; HD-WT compared to HD-HD, not significant [n.s.]). The WT-HD network is not significantly different from the WT-WT condition.

(C and D) Alteration in striatal pERK signaling of the HD-HD network is recapitulated in the HD-WT configuration.

(C) Quantification of pERK-positive cells after cortical stimulation shows a decrease in striatal signaling ($F_{3,94} = 22.2$, $p < 0.0001$; n = 25) in HD-HD and HD-WT networks (****p < 0.0001; HD-WT compared to HD-HD, n.s.), but not in WT-HD neurons.

(D) A dramatic decrease in pERK western blot signal ($F_{3,20} = 3.8$, $p < 0.05$; n = 6) is found in HD-HD and in HD-WT networks (*p < 0.05; HD-WT compared to HD-HD, n.s.), but not in WT-HD neurons.

(E–G) Quantifications GCaMP6f dynamics show alterations in neuronal activity and synchrony in HD-HD that are fully recapitulated in the HD-WT network.

(E) A similar decrease in the number of events per cells ($F_{3,2027} = 28.0$, $p < 0.0001$; n = 507) in HD-HD and HD-WT (*p < 0.05, ***p < 0.001, and ****p < 0.0001; HD-WT compared to HD-HD, n.s.) but a small increase in WT-HD neurons (*p < 0.05) are shown.

(F) A similar increase in amplitude of response ($F_{3,2027} = 57.2$, $p < 0.0001$) in HD-HD and HD-WT (****p < 0.0001; HD-WT compared to HD-HD, n.s.), but not in WT-HD neurons, is shown.

(G) A high proportion of highly synchronized events in HD-HD and HD-WT neurons (53.8% and 66.2%, respectively), but not in WT-WT and WT-HD neurons (42.5% and 36.5%, respectively), is shown. Error bar indicates SEM.

See also Figure S6.

Corticostriatal Activity Is Necessary and Sufficient to Induce Striatal Dysfunctions *In Vitro* and *In Vivo* in HD

Because of the contribution of the presynaptic compartment to HD dysfunctions, we directly assessed whether neuronal activity of cortical neurons is sufficient to induce alterations in the corticostriatal circuitry, both *in vitro* and *in vivo*. We took advantage of the fluidic isolation of the microchamber to selectively manipulate neuronal activity of cortical neurons with tetrodotoxin (TTX, a sodium channel blocker) while assessing network activity and synchrony (Figure 7A). As we previously observed, HD-HD networks treated with saline solution showed long episodes of silent activity interrupted by highly synchronized and massive bursting events, in clear contrast with the sparse and moderate activity in the WT-WT network (Figure 7B). Interestingly alterations in HD network activity and synchrony were dramatically decreased after TTX treatment of cortical neurons, as shown by the increased number of events, decreased amplitude, and lower proportion of synchronized events (Figures 7C–7E). These results suggest that abnormal cortical activity is necessary to induce aberrant corticostriatal connectivity in HD.

We next investigated whether cortical activity could drive *in vivo* alterations in striatal signaling responses using acute brain slices from WT and HD mice. Cortical projecting neurons from the layer V were electrically stimulated in acute horizontal brain slices from WT and *Hdh*$^{CAG140/+}$ mice preserving corticostriatal projections (Fino et al., 2005). Phospho-ERK signaling was then quantified using immunostaining in the corresponding projecting area of the striatum (Figure 7F). High-frequency stimulations of cortical neurons efficiently activated phospho-ERK signaling in the striatum, as shown by the increased number of phospho-ERK-positive neurons in the corresponding target area of the striatum (Figure 7G). In HD mice, the number

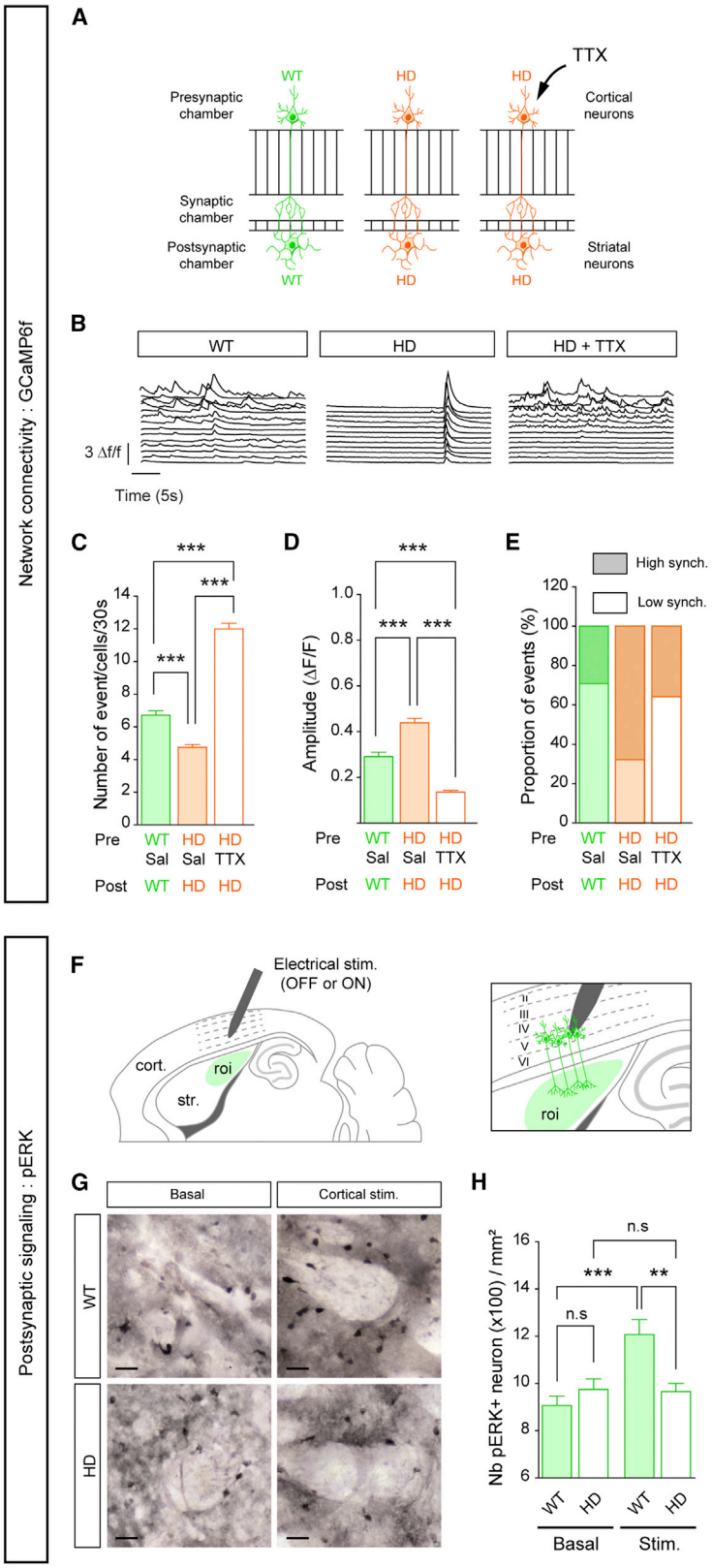

Figure 7. Striatal Consequences of Cortical Activity Manipulation *In Vitro* and *In Vivo* in HD

(A) Schematic showing the strategy for the selective inhibition of cortical activity using TTX. (B) Representative GCaMP6f traces obtained from WT and HD striatal neurons with or without cortical treatment with TTX.

(C–E) Quantifications of GCaMP6f dynamics show normal neuronal activity and synchrony in the HD network after cortical treatment with TTX. (C) Alterations in the number of events per cells (***$p < 0.0001$; $n = 480$), (D) amplitude of response per event (***$p < 0.0001$), and (E) the proportion of highly synchronized events in HD striatal neurons (WT, 29.1%; HD, 67.8%; HD + TTX, 35.7%) are rescued by cortical TTX.

(F–H) Cortical stimulations in acute brain slices induce impaired corticostriatal signaling in HD striatum.

(F) Schematic depicts the localization of electrical stimulations of layer V projecting neurons (ON) as well as the corresponding region of interest for pERK quantifications. In basal conditions, the electrode was placed but no stimulation was applied (OFF).

(G) Representative bright-field images show phospho-ERK-positive neurons in the striatum of WT and HD mice, in the basal condition and after cortical stimulation.

(H) Quantifications show an increased number of pERK-positive neurons after cortical stimulation in WT, but not HD, striatum *in vivo* ($F_{3,80} = 8.1$, $p < 0.0001$; $n = 21$; ***$p < 0.001$ and **$p < 0.01$; n.s., not significant). Error bar indicates SEM.

of phospho-ERK-positive striatal neurons was significantly decreased after cortical stimulations (Figure 7H), suggesting decreased corticostriatal connectivity and activity. We therefore conclude that cortical activity in HD is involved in corticostriatal network dysfunctions *in vitro* and *in vivo*. These results also suggest that cortical areas represent an important target to consider for therapeutic strategies.

DISCUSSION

Studying intracellular and synaptic dynamics *in vivo* is a challenge, although it is critical to better understand how distinct neuronal populations interact. The current challenge in studying cellular mechanisms within neurons is that *in vitro* cultures weakly recapitulate the physiology of neuron-to-neuron communication, especially within neurons of different identities. This is particularly important in the case of neurological disorders in which specific circuitries are damaged. Here we present an *in vitro* system compatible with high-resolution videomicroscopy, allowing the reconstruction and manipulation of functional and oriented neuronal networks that possess the characteristics of mature circuitry found *in vivo* (Figure S7). Using this original approach, we reconstructed an HD network *on-a-chip*, and we identified specific intracellular events that are selectively altered in disease.

Changes in Intracellular and Synaptic Dynamics in HD Depend on the Presynaptic Compartment

The HD corticostriatal circuit displayed marked changes to the dynamics of axonal vesicles. Defects in fast axonal transport appeared very early in the development of the network, and the alterations persisted even in the mature network. This suggests that the axonal transport defects in HD are probably an early pathogenic mechanism established during the development of neuronal circuits in the brain. Contrasting defects in axonal trafficking were observed for secretory vesicles and mitochondria, with vesicular dynamics progressively decreasing whereas mitochondrial motility increased. These changes in mitochondrial transport occurred at late stages of culture, when the circuit was mature, and they were correlated with an increase in the number of smaller mitochondria. These findings suggest that small, highly motile mitochondria are trafficked in the axons of HD neurons, contrary to the findings of previous studies reporting a decrease in mitochondrial trafficking (Chang et al., 2006; Orr et al., 2008; Trushina et al., 2004). However, these differences may result from the experimental conditions used. Indeed, short fragments of mutant huntingtin generating high levels of aggregates in axons and dendrites were used, and the authors linked the observed impairment of trafficking to the presence of aggregates. Nevertheless, abnormalities of both vesicular and mitochondrial motility may also predispose neurons to synapse dysfunction, as observed in neurons with syntaphilin mutations, in which mitochondrial motility increased due to anchoring impairment (Kang et al., 2008). Consistently, we observed a decrease in the density of corticostriatal synapses, with reduced BDNF-TrkB dynamics and glutamatergic transmission. These alterations may underlie the decrease in striatal signaling and basal neuronal activity, since both the BDNF-TrkB-signaling pathway and glutamatergic transmission have been shown to regulate downstream ERK signaling in striatal neurons (Baydyuk and Xu, 2014). Importantly, we found these alterations to occur specifically in the enkephalin-positive medium spiny projection neurons and prior to any cell death events, suggesting that our model recapitulates early events in disease.

Surprisingly, despite remaining silent most of the time, HD striatal neurons elicited sudden, exaggerated, and highly synchronized responses to spontaneous network activity (Figure 5). This hypersynchrony probably resulted from a dysregulation in neurotransmitter release at the presynaptic site that was sufficient to impair the full network. Consistent with this hypothesis, a previous study in a *Drosophila* model of HD reported an increase in Ca^{2+}-dependent neurotransmitter release, and it showed that reducing synaptic transmission via a partial loss of function of voltage-gated Ca^{2+} channels abolished both the electrophysiological and neurodegenerative phenotypes (Romero et al., 2008). These observations can be related to our findings showing altered synaptic connections and impaired excitatory glutamatergic transmission in HD (Figure 3). In fact, in both cases aberrant and large clusters were observed, suggesting dysfunctional and excessive release of excitatory neurotransmitter at presynaptic sites. Together, this corticostriatal hyperactivity may contribute to corticostriatal dysfunction and ultimately lead to neurodegeneration (Lewerenz and Maher, 2015).

This device allows one to manipulate the genetic status of pre- or postsynaptic neurons independently. Using this capacity, we showed that the nature of presynaptic neurons dominates the functionality of the whole network. Indeed, WT cortical neurons are sufficient to rescue network functionality and survival signaling in the HD striatum. Conversely, HD cortical neurons are sufficient to impair striatal signaling as well as the global functioning of the corticostriatal network. These findings are in agreement with a previous study (Zhao et al., 2016), and they have important implications for therapeutic strategies, as they support the notion that the cortex is a key structure in gene therapy approaches aiming to restore striatal function.

A Microfluidic Platform for Studying Multiple Brain Disorders

Given its versatility, the microfluidic platform can be used for almost any type of neuronal circuits or brain disorders. Here we challenged the system using a model of a neurodegenerative disorder by reconstructing a physiologically relevant corticostriatal network, such as the one that is affected in HD. We cultured corticostriatal projecting neurons (CTIP2/TBR1 positive) in the cortical chamber and output medium spiny neurons (enkephalin positive) in the striatal chamber. Using this system, we showed that the loss of correct corticostriatal connectivity can lead to unexpected consequences for striatal function, such as exaggerated and hypersynchronized responses to cortical signals. In addition, this network on-a-chip highlights the crucial role played by the presynaptic compartment in the sequence of events leading to striatum dysfunction and, ultimately, to degeneration. These results constitute a proof of concept for the utility of newly developed microfluidic systems for improving our understanding of the intracellular mechanisms

involved in the pathogenesis of brain disorders. Alternatively, other brain disorders involving hyperconnected networks, such as autism spectrum disorder (ASD) and/or attention deficit hyperactivity disorder (ADHD), could also be modeled. Microfluidic systems using cortical and striatal neurons from mouse models, such as SHANK3-knockout mice (Peça et al., 2011), could be used to determine the sequence of cellular dysfunctions leading to the defects in corticostriatal circuits typical of the disease. The combination of fluidic isolation and oriented neuronal connections would make it possible to trigger a primary pathogenic event in one identified compartment and to study the propagation of secondary dysfunctions in a controlled spatial and temporal environment.

In conclusion, we present a corticostriatal network on-a-chip using a microfluidic device suitable for high spatial and temporal resolution imaging. By applying this device to HD, we discovered unexpected cellular and network dysfunctions, highlighting the crucial role played by the cortical compartment in the genesis of striatal symptoms. This *on-a-chip* approach may prove to be useful for deciphering pathophysiological mechanisms and for validating drugs of therapeutic interest.

EXPERIMENTAL PROCEDURES

Further details and an outline of resources used in this work can be found in the Supplemental Experimental Procedures.

Mice

Hdh$^{CAG140/+}$ knockin mice were generated on a C57BL/6J background, and they express human *HTT* exon 1 sequence with 140 repeats of CAG, as described previously (Menalled et al., 2002). *Hdh*$^{Q111/+}$ knockin mice are generated on a CD1 background, and they express human *HTT* exon 1 sequence with 109 repeats of CAG, as described previously (Wheeler et al., 1999). Animals were maintained with access to food and water *ad libitum* and kept at a constant temperature (19°C –22°C) and humidity (40%–50%) on a 12:12-hr light/dark cycle. All experimental procedures were performed in an authorized establishment (Grenoble Institut des Neurosciences, INSERM U1216, license B3851610008) in strict accordance with the recommendations of the European Community (86/609/EEC) and the French National Committee (2010/63) for care and use of laboratory animals, under the supervision of authorized investigators (permission 91-448 to S. Humbert). Regarding controlled crosses, WT C57BL/6J or *Hdh*$^{CAG140/CAG140}$ male mice and WT CD1 or *Hdh*$^{Q111/Q111}$ male mice were mated, respectively, for one night with WT C57BL/6J or CD1 female mice.

Statistical Analyses

Statistical significance was determined using Prism5 (GraphPad). Synaptic transmission (iGluSnFR), postsynaptic signaling (pERK immunostaining, western blots, and immunochemistry), and network connectivity (GCaMP6f) were analyzed using one-way ANOVA followed by a Tukey post hoc test when more than two conditions were compared within a group (genotypes). Trafficking kinetics (BDNF-mCh and Mito-DsRed) were analyzed using two-way ANOVA followed by a Tukey post hoc test when comparing more than 2 variables (DIV and genotypes). Synaptic formation (SYN/PSD95 and VGLUT1/PSD95), synaptic transmission (iGluSnFR), trafficking kinetics (TrkB-mCh), size classification (Mito-DsRed, iGluSnFR, and SYN), postsynaptic signaling (pERK immunostaining and western blot), mitochondrial function (TMRM), and network connectivity (GCaMP6f) were analyzed using unpaired two-tailed Student's t tests when only two conditions were compared within a group (WT versus HD). The distributions of motile vesicles (BDNF-mCh) and synchrony (GCaMP6f) were analyzed using a Pearson's chi-square test. Results are expressed as mean ± SEM. The criterion for statistical significance was set at $p < 0.05$.

SUPPLEMENTAL INFORMATION

Supplemental Information includes Supplemental Experimental Procedures, seven figures, and five movies and can be found with this article online at https://doi.org/10.1016/j.celrep.2017.12.013.

ACKNOWLEDGMENTS

We thank S. Humbert and M. Kreutz for support and critical reading of the manuscript and members of the Saudou and Humbert labs for discussions; Y. Saoudi and the imaging facility platform (PIC-GIN) for help with image acquisitions; C. Scaramuzzino for providing confocal images; C. Benstaali for mouse care; E. Valjent, P. Trifilieff, M. Barnat, and T. Honegger for technical advice; and G. Froment, D. Nègre, and C. Costa from the lentivirus production facility of SFR Biosciences (UMS3444/CNRS, US8/INSERM, ENS de Lyon, UCBL). This work was supported by grants from Agence Nationale pour la Recherche (ANR-12-BLAN-SVSE2 and ANR-14-CE35-0027-01, F.S.; ANR-12-PDOC-0004-01, M.C.), Fondation pour la Recherche Médicale (FRM, équipe labellisée, F.S.), Fondation Bettencourt Schueller (F.S.), Fédération pour la Recherche sur le Cerveau (F.S.), INSERM (F.S. and M.C.), AGEMED program (F.S.), and NeuroCoG in the framework of the "Investissements d'avenir" program (ANR-15-IDEX-02). The F.S. laboratory is a member of the Grenoble Center of Excellence in Neurodegeneration (GREEN). A.V. was supported by a PhD fellowship from DIM "Cerveau et Pensée" and FRM (FDT2016043504).

AUTHOR CONTRIBUTIONS

Conceptualization, A.V., B.C., M.C., and F.S.; Methodology, A.V., E.M., W.C., J.B., E.F., B.C., M.C., and F.S.; Investigation, A.V., E.M., W.C., A.G., E.F., and M.C.; Formal Analysis, A.V., E.M., W.C., M.C., and F.S.; Writing – Original Draft, A.V., B.C., M.C., and F.S.; Writing – Review & Editing, A.V., E.M., W.C., A.G., J.B., E.F., B.C., M.C., and F.S.; Funding Acquisition, M.C. and F.S.; Supervision, M.C. and F.S.

DECLARATION OF INTERESTS

The authors declare no competing interests.

Received: July 4, 2017
Revised: November 1, 2017
Accepted: December 1, 2017
Published: January 2, 2018

REFERENCES

Baydyuk, M., and Xu, B. (2014). BDNF signaling and survival of striatal neurons. Front. Cell. Neurosci. *8*, 254.

Borrell-Pagès, M., Canals, J.M., Cordelières, F.P., Parker, J.A., Pineda, J.R., Grange, G., Bryson, E.A., Guillermier, M., Hirsch, E., Hantraye, P., et al. (2006). Cystamine and cysteamine increase brain levels of BDNF in Huntington disease via HSJ1b and transglutaminase. J. Clin. Invest. *116*, 1410–1424.

Brito, V., Giralt, A., Enriquez-Barreto, L., Puigdellívol, M., Suelves, N., Zamora-Moratalla, A., Ballesteros, J.J., Martín, E.D., Dominguez-Iturza, N., Morales, M., et al. (2014). Neurotrophin receptor p75(NTR) mediates Huntington's disease-associated synaptic and memory dysfunction. J. Clin. Invest. *124*, 4411–4428.

Buren, C., Parsons, M.P., Smith-Dijak, A., and Raymond, L.A. (2016). Impaired development of cortico-striatal synaptic connectivity in a cell culture model of Huntington's disease. Neurobiol. Dis. *87*, 80–90.

Cepeda, C., Hurst, R.S., Calvert, C.R., Hernández-Echeagaray, E., Nguyen, O.K., Jocoy, E., Christian, L.J., Ariano, M.A., and Levine, M.S. (2003). Transient and progressive electrophysiological alterations in the corticostriatal pathway in a mouse model of Huntington's disease. J. Neurosci. *23*, 961–969.

Chang, D.T., Rintoul, G.L., Pandipati, S., and Reynolds, I.J. (2006). Mutant huntingtin aggregates impair mitochondrial movement and trafficking in cortical neurons. Neurobiol. Dis. *22*, 388–400.

Chen, T.W., Wardill, T.J., Sun, Y., Pulver, S.R., Renninger, S.L., Baohan, A., Schreiter, E.R., Kerr, R.A., Orger, M.B., Jayaraman, V., et al. (2013). Ultrasensitive fluorescent proteins for imaging neuronal activity. Nature *499*, 295–300.

Chiappalone, M., Bove, M., Vato, A., Tedesco, M., and Martinoia, S. (2006). Dissociated cortical networks show spontaneously correlated activity patterns during in vitro development. Brain Res. *1093*, 41–53.

Costa, V., Giacomello, M., Hudec, R., Lopreiato, R., Ermak, G., Lim, D., Malorni, W., Davies, K.J., Carafoli, E., and Scorrano, L. (2010). Mitochondrial fission and cristae disruption increase the response of cell models of Huntington's disease to apoptotic stimuli. EMBO Mol. Med. *2*, 490–503.

Digilio, L., Yap, C.C., and Winckler, B. (2015). Ctip2-, Satb2-, Prox1-, and GAD65-Expressing Neurons in Rat Cultures: Preponderance of Single- and Double-Positive Cells, and Cell Type-Specific Expression of Neuron-Specific Gene Family Members, Nsg-1 (NEEP21) and Nsg-2 (P19). PLoS ONE *10*, e0140010.

Estrada-Sánchez, A.M., Burroughs, C.L., Cavaliere, S., Barton, S.J., Chen, S., Yang, X.W., and Rebec, G.V. (2015). Cortical efferents lacking mutant huntingtin improve striatal neuronal activity and behavior in a conditional mouse model of Huntington's disease. J. Neurosci. *35*, 4440–4451.

Fino, E., Glowinski, J., and Venance, L. (2005). Bidirectional activity-dependent plasticity at corticostriatal synapses. J. Neurosci. *25*, 11279–11287.

Gatto, R.G., Chu, Y., Ye, A.Q., Price, S.D., Tavassoli, E., Buenaventura, A., Brady, S.T., Magin, R.L., Kordower, J.H., and Morfini, G.A. (2015). Analysis of YFP(J16)-R6/2 reporter mice and postmortem brains reveals early pathology and increased vulnerability of callosal axons in Huntington's disease. Hum. Mol. Genet. *24*, 5285–5298.

Gauthier, L.R., Charrin, B.C., Borrell-Pagès, M., Dompierre, J.P., Rangone, H., Cordelières, F.P., De Mey, J., MacDonald, M.E., Lessmann, V., Humbert, S., and Saudou, F. (2004). Huntingtin controls neurotrophic support and survival of neurons by enhancing BDNF vesicular transport along microtubules. Cell *118*, 127–138.

Her, L.S., and Goldstein, L.S. (2008). Enhanced sensitivity of striatal neurons to axonal transport defects induced by mutant huntingtin. J. Neurosci. *28*, 13662–13672.

Hinckelmann, M.V., Virlogeux, A., Niehage, C., Poujol, C., Choquet, D., Hoflack, B., Zala, D., and Saudou, F. (2016). Self-propelling vesicles define glycolysis as the minimal energy machinery for neuronal transport. Nat. Commun. *7*, 13233.

Kang, J.S., Tian, J.H., Pan, P.Y., Zald, P., Li, C., Deng, C., and Sheng, Z.H. (2008). Docking of axonal mitochondria by syntaphilin controls their mobility and affects short-term facilitation. Cell *132*, 137–148.

Lewerenz, J., and Maher, P. (2015). Chronic Glutamate Toxicity in Neurodegenerative Diseases-What is the Evidence? Front. Neurosci. *9*, 469.

Liot, G., Zala, D., Pla, P., Mottet, G., Piel, M., and Saudou, F. (2013). Mutant Huntingtin alters retrograde transport of TrkB receptors in striatal dendrites. J. Neurosci. *33*, 6298–6309.

Marvin, J.S., Borghuis, B.G., Tian, L., Cichon, J., Harnett, M.T., Akerboom, J., Gordus, A., Renninger, S.L., Chen, T.W., Bargmann, C.I., et al. (2013). An optimized fluorescent probe for visualizing glutamate neurotransmission. Nat. Methods *10*, 162–170.

McKinstry, S.U., Karadeniz, Y.B., Worthington, A.K., Hayrapetyan, V.Y., Ozlu, M.I., Serafin-Molina, K., Risher, W.C., Ustunkaya, T., Dragatsis, I., Zeitlin, S., et al. (2014). Huntingtin is required for normal excitatory synapse development in cortical and striatal circuits. J. Neurosci. *34*, 9455–9472.

Menalled, L.B., Sison, J.D., Wu, Y., Olivieri, M., Li, X.J., Li, H., Zeitlin, S., and Chesselet, M.F. (2002). Early motor dysfunction and striosomal distribution of huntingtin microaggregates in Huntington's disease knock-in mice. J. Neurosci. *22*, 8266–8276.

Orr, A.L., Li, S., Wang, C.E., Li, H., Wang, J., Rong, J., Xu, X., Mastroberardino, P.G., Greenamyre, J.T., and Li, X.J. (2008). N-terminal mutant huntingtin associates with mitochondria and impairs mitochondrial trafficking. J. Neurosci. *28*, 2783–2792.

Peça, J., Feliciano, C., Ting, J.T., Wang, W., Wells, M.F., Venkatraman, T.N., Lascola, C.D., Fu, Z., and Feng, G. (2011). Shank3 mutant mice display autistic-like behaviours and striatal dysfunction. Nature *472*, 437–442.

Plotkin, J.L., Day, M., Peterson, J.D., Xie, Z., Kress, G.J., Rafalovich, I., Kondapalli, J., Gertler, T.S., Flajolet, M., Greengard, P., et al. (2014). Impaired TrkB receptor signaling underlies corticostriatal dysfunction in Huntington's disease. Neuron *83*, 178–188.

Romero, E., Cha, G.H., Verstreken, P., Ly, C.V., Hughes, R.E., Bellen, H.J., and Botas, J. (2008). Suppression of neurodegeneration and increased neurotransmission caused by expanded full-length huntingtin accumulating in the cytoplasm. Neuron *57*, 27–40.

Rosas, H.D., Lee, S.Y., Bender, A.C., Zaleta, A.K., Vangel, M., Yu, P., Fischl, B., Pappu, V., Onorato, C., Cha, J.H., et al. (2010). Altered white matter microstructure in the corpus callosum in Huntington's disease: implications for cortical "disconnection". Neuroimage *49*, 2995–3004.

Ross, C.A., and Tabrizi, S.J. (2011). Huntington's disease: from molecular pathogenesis to clinical treatment. Lancet Neurol. *10*, 83–98.

Saudou, F., and Humbert, S. (2016). The Biology of Huntingtin. Neuron *89*, 910–926.

Scaduto, R.C., Jr., and Grotyohann, L.W. (1999). Measurement of mitochondrial membrane potential using fluorescent rhodamine derivatives. Biophys. J. *76*, 469–477.

Song, W., Chen, J., Petrilli, A., Liot, G., Klinglmayr, E., Zhou, Y., Poquiz, P., Tjong, J., Pouladi, M.A., Hayden, M.R., et al. (2011). Mutant huntingtin binds the mitochondrial fission GTPase dynamin-related protein-1 and increases its enzymatic activity. Nat. Med. *17*, 377–382.

Tabrizi, S.J., Scahill, R.I., Durr, A., Roos, R.A., Leavitt, B.R., Jones, R., Landwehrmeyer, G.B., Fox, N.C., Johnson, H., Hicks, S.L., et al.; TRACK-HD Investigators (2011). Biological and clinical changes in premanifest and early stage Huntington's disease in the TRACK-HD study: the 12-month longitudinal analysis. Lancet Neurol. *10*, 31–42.

Taylor, A.M., Blurton-Jones, M., Rhee, S.W., Cribbs, D.H., Cotman, C.W., and Jeon, N.L. (2005). A microfluidic culture platform for CNS axonal injury, regeneration and transport. Nat. Methods *2*, 599–605.

Taylor, A.M., Dieterich, D.C., Ito, H.T., Kim, S.A., and Schuman, E.M. (2010). Microfluidic local perfusion chambers for the visualization and manipulation of synapses. Neuron *66*, 57–68.

Trushina, E., Dyer, R.B., Badger, J.D., 2nd, Ure, D., Eide, L., Tran, D.D., Vrieze, B.T., Legendre-Guillemin, V., McPherson, P.S., Mandavilli, B.S., et al. (2004). Mutant huntingtin impairs axonal trafficking in mammalian neurons in vivo and in vitro. Mol. Cell. Biol. *24*, 8195–8209.

Wang, N., Gray, M., Lu, X.H., Cantle, J.P., Holley, S.M., Greiner, E., Gu, X., Shirasaki, D., Cepeda, C., Li, Y., et al. (2014). Neuronal targets for reducing mutant huntingtin expression to ameliorate disease in a mouse model of Huntington's disease. Nat. Med. *20*, 536–541.

Wheeler, V.C., Auerbach, W., White, J.K., Srinidhi, J., Auerbach, A., Ryan, A., Duyao, M.P., Vrbanac, V., Weaver, M., Gusella, J.F., et al. (1999). Length-dependent gametic CAG repeat instability in the Huntington's disease knock-in mouse. Hum. Mol. Genet. *8*, 115–122.

Zhao, X., Chen, X.Q., Han, E., Hu, Y., Paik, P., Ding, Z., Overman, J., Lau, A.L., Shahmoradian, S.H., Chiu, W., et al. (2016). TRiC subunits enhance BDNF axonal transport and rescue striatal atrophy in Huntington's disease. Proc. Natl. Acad. Sci. USA *113*, E5655–E5664.

Zuccato, C., Valenza, M., and Cattaneo, E. (2010). Molecular mechanisms and potential therapeutical targets in Huntington's disease. Physiol. Rev. *90*, 905–981.